Hydrol. Earth Syst. Sci. Discuss., 11, 2233–2262, 2014
www.hydrol-earth-syst-sci-discuss.net/11/2233/2014/
doi:10.5194/hessd-11-2233-2014

Hydrology and Earth System Sciences
Discussions

Simulating the connections of ENSO and the hydrology of the Blue Nile using a climate model of the tropics

M. A. H. Zaroug[1,2], **F. Giorgi**[1], **E. Coppale**[1], **and E. A. B. Eltahir**[3]

[1]International Center for Theoretical Physics, Earth System Physics, Trieste, Italy
[2]Dinder Center for Environmental Research, Khartoum, Sudan
[3]Massachusetts Institute of Technology, Civil and Environmental Engineering, Cambridge, USA

Received: 18 December 2013 – Accepted: 5 January 2014 – Published: 20 February 2014

Correspondence to: M. A. H. Zaroug (modathir_23@yahoo.com)

Published by Copernicus Publications on behalf of the European Geosciences Union.

Abstract

We simulate the observed statistical relationship between ENSO and the hydrology of the Blue Nile using the tropical-band version of the regional climate model RegCM4 (or Reg-TB) for the 28 yr period 1982–2009. An ensemble of 9 simulations is completed to investigate the role of ENSO in the hydrology of the Blue Nile catchment. Re-TB shows a good skill in simulating the climatology of temperature, outgoing long-wave radiation patterns as well as related atmospheric circulation features during the summer season (i.e. the rainy season over the Blue Nile catchment). The model also succeeds in reproducing the observed negative correlation between Pacific SST and rainfall anomalies over the Blue Nile catchment, and in particular the association of droughts over the Blue Nile with El Niño events that start during the April–June period. We thus propose that observations as well as model forecasts of Pacific SST during this season should be used in seasonal forecasting of the Blue Nile flow.

1 Introduction

The Blue Nile has a great impact on the life of millions of people in Ethiopia, Sudan, and Egypt. It originates from Lake Tana and descends from the Ethiopian high plateau, with many tributaries in its upper course across the Ethiopian Highlands and two more tributaries (Dinder and the Rahad) in its lower course across Sudan. Although the Blue Nile is relatively short compared to the White Nile and it has a relatively small drainage area, it carries 60–70 % of the total discharge and a great amount of sediment (Dumont, 2009).

During the last few decades, there has been a wide recognition that natural oscillations in the state of the Pacific Ocean have a significant impact on the patterns of weather and climate around the world. The dominant among these oscillations is known as the El Niño – Southern Oscillation (ENSO) which has a period of about 4 yr. ENSO is the largest contributor to inter-annual climate variability in the tropical

HESSD
11, 2233–2262, 2014

Pacific as well as in remote regions around the globe (e.g. Müller and Roeckner, 2008). Eltahir (1996) found that 25 % of the natural variability in the annual flow of the Nile is associated with ENSO and proposed to use this observed correlation to improve the predictability of the Nile floods. Wang and Eltahir (1999) recommended an empirical methodology for medium and long-range (~6 months) forecasting of the Nile floods using ENSO information, while Amarasekera et al. (1997) showed that ENSO episodes are negatively correlated with the floods of the Blue Nile and Atbara rivers which originate in Ethiopia. In addition, Eltahir (1996) showed that the probability of having a low (high) flood given cold SST conditions is 2 % (49 %), while the probability of having a high (low) flood given a warm SST condition is 8 % (58 %).

Some recent studies divided Ethiopia into regions according to the variability of rainfall seasonality and used observational datasets to study the impact of sea surface temperature (SST) on the rainfall in the Ethiopian Highlands (Segele and Lamb, 2005; Seleshi and Zanke, 2004; Gissila et al., 2004). Other studies concentrated on East Africa but in regions outside the Ethiopian Highland, and showed negative correlation with ENSO in central and southern Sudan (Osman et al., 2001; Elagib and Elhag, 2011; Osman and Shamseldin, 2002).

These previous studies were conducted using observational datasets of SST, rainfall and river flow. In this study, we assess whether these observed connections between droughts/floods in the Blue Nile region and SSTs in the Pacific Ocean can be reproduced by using a physically based model of the climate system (the Regional Climate Model RegCM4 in its tropical band configuration, RegTB; Giorgi et al., 2012; Coppola et al., 2012). Towards this purpose we completed and analysed an ensemble of 9 simulations of tropical climate driven by observed SSTs and north-south boundary conditions from the ERA-Interim reanalysis of observations for the 28-yr period 1982–2009. In particular, we focus on the impact of ENSO on drought and flood conditions in the upper catchment of the Blue Nile by comparing simulation results with available discharge and precipitation observations.

HESSD
11, 2233–2262, 2014

In Sect. 2 we describe model and experiment design, while in Sect. 3 we validate the model climatology over the Africa region of interest in this study. In Sect. 4 we then assess the representation of the connections between ENSO and the flood/drought conditions in the Blue Nile river basin. Final considerations are then provided in Sect. 5.

2 REGCM4 description, experiments and data

RegCM4 is described by Giorgi et al. (2012). It is an evolution of the previous version, RegCM3, described by Pal et al., (2007), with multiple physics options. Among the new developments of RegCM4 is the tropical band configurations described by Coppola et al. (2012), or Reg-TB, by which the model domain covers the entire tropical belt with periodic boundary conditions in the x direction and relaxation boundary conditions at the southern and northern boundaries. Figure 1 shows the model domain and topography along with some sub-regions selected for more detailed regional analysis. For our experiments the horizontal resolution is approximately 125 km at the equator, i.e. 360 grid points. In the north-south direction the domain extends to about +/−45 degrees and 18 sigma layers are used in the vertical, as in its standard configuration. The red rectangle in the Pacific Ocean represents the Nino 3.4 region, whereas the small square over Ethiopia represents out study area, i.e. the catchment of the upper Blue Nile.

For our experiment we used the following physics options described in Giorgi et al. (2012): modified CCM3 radiative transfer scheme (Kiehl et al., 1996), modified (Holtslag et al., 1990) planetary boundary layer scheme, SUBEX resolvable precipitation scheme (Pal et al., 2000), mixed cumulus convection configuration utilizing the scheme of Grell (1993) over land and that of (Emanuel, 1991) over oceans and the biosphere–atmosphere transfer scheme (Dickinson et al., 1993) land surface package. As mentioned, the model uses forcing lateral boundary conditions only in the northern and southern boundaries of the domain, with no external forcing in an east–west direction. The initial and lateral boundary conditions are provided by

HESSD
11, 2233–2262, 2014

the ERA-Interim 1.5° × 1.5° gridded reanalysis (ERAI, Dee et al., 2011) which is the third generation ECMWF reanalysis product. SSTs are from the weekly, 1° resolution Optimum Interpolation (OI) SST dataset from the national Oceanic and Atmospheric Administration (Reynolds et al., 2007). The simulation period is from 1 January 1982 to 31 March 2010 (28 yr) and 9 ensemble members are completed. The observed data used for model validation is the Global Precipitation Climatology Project (GPCP) version 2.2 (Huffman et al., 2011) available from January 1979 to December 2010 with a resolution of 2.5°. The Climate Research Unit (CRU, land only, 0.5° × 0.5° resolution; Mitchell et al., 2004) is also used for more detailed regional analysis.

3 Validation of model climatology over East Africa

In this section we first present a basic validation of the model climatology during the June-July-August-September (JJAS) rainy season over the broad east Africa region by comparing averages taken over the entire nine member ensemble with available observations. Note that this model configuration is the same as that used by Coppola et al. (2012), and in that paper an assessment is provided of the model climatology over the entire tropical belt. In this regard, Coppola et al. (2012) show that, although regional biases in the model are present, the basic model climatology of equatorial and tropical regions is realistic. We also recall that, although we only analyse here data from the African region, the model is run for the full tropical band with forcing only at the northern and southern boundary, and therefore it is quite free to develop its own regional circulations within this large domain.

3.1 Rainfall

The spatial pattern of JJAS rainfall is compared to observations (both CRU and GPCP) in Fig. 2. In JJAS the ITCZ is located in the northern hemisphere, therefore rainfall over the continent is mostly confined between 7° S and 18° N, while regions above and

HESSD
11, 2233–2262, 2014

below these latitudes are relatively dry. This pattern of rainfall is mainly associated with the occurrence of mesoscale convective systems (d'Amato and Lebel, 1998; Jenkins et al., 2005). Two rainfall maxima are located around the Cameroon Mountains and Ethiopian Highlands which are associated with local orographic features. The model captures the general patterns of the observed rainfall distribution, in particular the ITCZ position and intensity. However, rainfall over southern Sudan, Central Africa and the Ethiopian Highlands is overestimated. Also, the monsoon rain belt appears narrower in the model than in the observational datasets, as indicated by the negative precipitation biases north and south of the main rain belt. In general, the performance of our Reg-TB configuration appears in line with previous studies performed using the RegCM system in various configurations and domains (Sun et al., 1999; Pal et al., 2007; Anyah and Semazzi, 2007; Sylla et al., 2010b; Steiner et al., 2009; Zaroug et al., 2013) or other regional modeling systems (e.g., Vizy and Cook, 2002; Nikulin et al., 2012; Paeth et al., 2005; Gallée et al., 2004; Flaounas et al., 2011; Druyan et al., 2008).

3.2 Temperature

The seasonal average of JJA 2-m temperature for 1982–2009 is compared to CRU observations in Fig. 3. The lowest temperatures are found mostly over the mountainous areas of Cameroun and Ethiopian Highlands, Tanzania and south Kenya, while the warmest areas are confined between 15 and 27° N, with larger values over the Sahara desert. Reg-TB (Fig. 3a) reproduces this spatial pattern but it shows a systematic cold bias of a few degrees in the convective regions in East Africa (Fig. 3b), Nigeria, Algeria, and Libya. This cold bias over tropical and equatorial Africa has been a persistent feature in RegCM, as also found for example in the experiments of Sylla et al. (2010b) and Coppola et al. (2012), although the magnitude of the bias is somewhat reduced in our simulation. It should be stressed that the CRU observations are possibly affected by large uncertainties in this region due to the lack of observing stations, particularly in remote and mountainous areas (Mitchell et al., 2004). In addition, surface temperature depends on many parameters, including the presence of dust and aerosols. Given the

HESSD
11, 2233–2262, 2014

uncertainty about these variables and that we do not include such processes in the model, we assess that a model bias of a few degrees is acceptable for this study.

3.3 Outgoing Longwave Radiation (OLR)

Figure 4 compares simulated and observed (NOAA) averaged JJA OLR, which is essentially a measure of cloudiness. Both the model (Fig. 4a) and the observations (not shown) exhibit larger OLR values in North Africa and south of 5° S because of small amounts of cloud cover, with correspondingly low OLR over the ITCZ. The model tends to overestimate the OLR over the Congo basin as a result of an underestimation of clouds over this region, a result which is in line with previous applications of thee model (Zaroug et al., 2013; Sylla et al., 2010a, b). Slight overestimates are found over the Sahara and the greater horn of Africa, but in general the model captures well the general observed features of the OLR pattern in both magnitude and spatial extent.

3.4 Low level circulation, Tropical Easterly Jet (TEJ) and African Easterly Jet (AEJ)

The spatial patterns of average JJA low level (925 mb) circulation are shown in Fig. 5a for the ERA Interim reanalysis and Fig. 5b for the RegTB simulation. Direct observations of the low level wind over the region are not available, and thus we use here the reanalysis product for evaluating the model. Overall, the model reproduces well the main features of the low level circulation, such as the low level monsoon flow over North Africa, the northerly Harmattan flow over East Africa, and the southeasterly flow over the Horn of Africa.

The TEJ develops between 200 and 150 mb in the upper troposphere over India in response to a large meridional thermal gradient and settles during the northern summer Asian monsoon season between the Tibetan Highlands and the Indian Ocean (Fontaine and Janicot, 1992; Koteswaram, 1958; Chen and van Loon, 1987). It stretches from the Indochina peninsula, across the African continent, to the tropical

HESSD
11, 2233–2262, 2014

Atlantic (Wu et al., 2009), and it is linked to anomalous SSTs on a planetary scale (Chen and van Loon, 1987). The TEJ is one of the planetary features that affect the north African summer climate variability (Chen and van Loon, 1987). Figure 6a shows the TEJ in the ERA Interim reanalysis confined between 3 and 17° N with a core speed exceeding 15 m s^{-1}. The band of the jet decreases gradually from East Africa to West Africa. In fact, the highest wind speed of about 18 m s^{-1} occurs over the Horn of Africa and the western Indian Ocean, while the lowest values of about 6 m s^{-1} are found over Niger. RegTB reproduces well the structure of the TEJ shown in the ERA Interim reanalysis, capturing both the location and intensity of the jet, although the core of the jet extends somewhat westward and further into Sudan compared to ERA-Interim.

The AEJ results mainly from the vertical inversion (around 600–700 mb) of the meridional temperature gradient between the Sahara and equatorial Africa due to the existence of strong surface baroclinicity (Cook, 1999; Steiner et al., 2009) associated with atmospheric deep convection (Thorncroft and Blackburn, 1999; Sylla et al., 2010b). Figure 6c shows the ERA Interim zonal wind in JJA at 600 mb. It is confined approximately between 7 and 20° N extending from Chad to the Atlantic Ocean with a core speed ranging from 11 to 13 m s^{-1} located over West Africa. Again, RegTB simulates reasonably well both the strength and location of the AEJ (Fig. 6d).

In summary, the analysis presented in this section indicates that RegTB produces a realistic simulation of the climatology of the main dynamical and thermodynamical features of East African climate. In the next section we can thus turn our attention to the connections between ENSO and the hydroclimate of the upper Nile river basin.

4 ENSO Connections with East African Climate

4.1 Difference between La Niña and El Niño years

Figure 7 provides an assessment of the capability of the observational GPCP dataset to captures the differences in East African climate between La Niña and El Niño years.

HESSD
11, 2233–2262, 2014

The GPCP data was analyzed for 28 yr (1982–2009), and then 5 La Niña years and 5 El Niño years included in this period were selected. The average precipitation for the 5 La Niña years (1988, 1998, 1999, 2007, and 2008), the 5 El Niño years (1982, 1983, 1987, 1992, and 2002) along with their difference are shown in the upper, middle and lower panels of Fig. 7, respectively. The GPCP data show a strong signal of increased rainfall during La Niña years over the Sahel region up to about 18° N, including the upper catchment of the Nile river. This result agrees qualitatively with previous observational analyses, which suggested that La Niña years are associated with above normal rainfall and El Niño years with below normal rainfall in the upper catchment of the Blue Nile (Eltahir, 1996; Wang and Eltahir, 1999; Amarasekera et al., 1997; De Putter et al., 1998; Camberlin et al., 2001; Abtew et al., 2009).

Figure 8 shows the corresponding fields for the 9 member ensemble of RegTB simulations. The 9 members were averaged over the 28 simulated years (1982–2009), and then 5 La Niña years and 5 El Niño years were selected as in the observational analysis. It can be seen that the model captures the positive La Niña minus El Niño precipitation signal over the Sahel region, although this is less intense than in the observations and does not extend as faar north. In addition, the models show a negative signal in the region just North of Lake Victoria. The results of each ensemble member were also analyzed (not shown) and they showed a remarkable variability between different members, which results in the main signal over the Sahel being weakened. Notwithstanding this problem, it appears that the model captured the main positive signal over the Sahel band and the upper Nile catchment.

4.2 Correlation between rainfall anomalies over the Ethiopian Highlands and SST anomalies over the Pacific Ocean In the Nino 3.4 region

Figure 9 shows the correlation between the ensemble average rainfall anomalies over the upper Nile river catchment (see box in Fig. 1) during JJAS and the SST anomalies in the Nino 3.4 region during three month periods from January-February-March (JFM) to October-November-December (OND). The correlations are negative for all SST

HESSD
11, 2233–2262, 2014

seasons, with the highest value of −0.62 during AMJ and the lowest of −0.35 in OND. Figure 10 shows the time evolution of AMJ SST anomalies and ensemble average JJAS precipitation over the upper Blue Nile river catchment, further evidencing the negative correlation between these two variables.

In a recent study Zaroug et al. (2013) showed that the Blue Nile river discharge showed the highest correlation for drought events with the Nino 3.4 SST during AMJ, a result which appears to be in line with those of Figs. 9 and 10. These results support the use of Nino 3.4 SST during AMJ for seasonal forecasting of hydroclimate conditions in the upper catchment of the Blue Nile. While the correlations of Fig. 9 were calculated using the 9 member ensemble average, we also repeated the same exercise for each member separately (not shown) and found lower correlation values and a wide spread across members. This indicates that ensembles of simulations are needed to capture the atmospheric response to ENSO (Shukla et al., 2000).

4.3 Regression analysis of DJF and JJA Nino 3.4 index onto REGCM rainfall

In this section we investigate further the relationship through the regression analysis between SST in the Nino 3.4 region for different seasons (DJF and JJA), and the GPCP and model rainfall. The upper panel of Fig. 8 presents the regression of DJF Nino 3.4 index onto the DJF GPCP rainfall from 1982 to 2009, while the lower panel of Fig. 8 shows the same regression for JJA. Nino 3.4 has an impact on many regions around the world. During DJF it has a high positive signal in the equatorial Pacific as shown in Fig. 11a, Kenya and Tanzania shows also to a less extend a positive signal. On the other hand, the southern countries of Africa, Amazon Basin and western equatorial Pacific shows negative signal. In Fig. 11b during JJA, the positive signal in the equatorial Pacific becomes narrower. The negative signal extends along the Sahel region and below up to the equator. The India, and south east Asia and northern part of South America shows a negative signal.

The same regression analysis focusing on the East Africa region is shown in Fig. 12. We find a positive signal over Kenya showed during DJF a positive signals of regression

HESSD
11, 2233–2262, 2014

analysis as shown in Fig. 12a. In Fig. 12b almost the whole ITCZ during JJA showed negative correlation. The Ethiopian Highland showed the highest negative correlation in Africa.

The same analysis was performed on the ensemble mean for the two seasons (DJF and JJA) as shown in Fig. 13. The model results agree with the observational based regression, showing no effect on the rainfall during the low flow season in the upper catchment of the Blue Nile as shown in the top panel of Fig. 10. The model manages to simulate during DJF the positive signal in the equatorial Pacific and east Africa as shown in Fig. 13a. The model also shows positive signal in the Congo Basin. It captured to a less extend the negative signal in the Amazon Basin and the west most of the equatorial Pacific (Fig. 13a). The lower panel of Fig. 10 shows a negative signal of the regression in Ethiopian Highland during JJA (around −1). However the band and the length of the negative regression is small compare to the observational based results in Africa. The model manages also in Fig. 13b to capture the negative signal in the Indian peninsula. Figure 11 shows the same analysis in Fig. 10. It shows a magnified picture for North Africa for the regression of Nino 3.4 onto the 9 averaged members' rainfall in North Africa for DJF and JJA. Part of Kenya, and part of Uganda and the Congo Basin showed positive signals during DJF as shown in Fig. 11a, the Ethiopian highland and central Sudan showed negatives signals.

5 Conclusions

In this study we use the tropical band version of the RegCM4 system (Giorgi et al., 2012; Coppola et al., 2012) to simulate the observed statistical relationship between ENSO and the hydrology of the Blue Nile. Towards this objective a series of 9 28-yr long simulations were completed for a domain covering the entire tropical belt between ~45° S and ~45° N, driven by observed SST and north-south boundary conditions from the ERA-Interim reanalysis.

HESSD
11, 2233–2262, 2014

The RegTB is first evaluated against observations and the reanalysis product over the East Africa region. It is shown that the model performs reasonably well in reproducing the observed climatology of temperature, rainfall, outgoing long wave radiation and large scale atmospheric circulation features. For example, the model captures well the rain belt, as well as the peaks in Ethiopian Highlands, Guinea Highlands, and Cameron Highlands. In general, the temperature biases are approximately between −2 and 2 °C. In fact, this simulation outperforms in some aspects the previous application of this model over the region (Sylla et al., 2010b; Zaroug et al., 2013). In addition, the lower level and large-scale circulation features affecting the monsoon (TEJ, AEJ) are realistically captured.

We then analyse the ability of the model to reproduce the observed connections between Pacific SST and precipitation over the upper Nile River catchment. The model (average of 9 members) was able to reproduce the observed negative correlation between Nino 3.4 SST and upper Nile precipitation, and showed the highest correlation during AMJ (−0.62), in line with previous observational studies (Zaroug et al., 2013). It suggests that AMJ SSTs over the Nino 3.4 region can be a useful predictor in seasonal (JJAS) precipitation forecasting over the East Afrca and Blue Nile river region. Our analysis provides encouraging indications towards the use of the RegTB configuration in seasonal forecasting, climate change and teleconnection studies over thee broas East Africa region.

Acknowledgements. This work has been supported by the Earth System Physics (ESP) in the International Centre for Theoretical Physics (ICTP), the STEP program and the EU funded collaborative DEWFORA project. The author would like to acknowledge Dr. Fred Kucharski for his support in sharing his modelling experience. Finally, I would like to thank all the staff of the ESP for their support.

HESSD
11, 2233–2262, 2014

References

Abtew, W., Melesse, A. M., and Dessalegne, T.: El Niño Southern Oscillation link to the Blue Nile River Basin hydrology, Hydrol. Process., 23, 3653–3660, 2009.

Amarasekera, K. N., Lee, R. F., Williams, E. R., and Eltahir, E. A. B.: ENSO and the natural variability in the flow of tropical rivers, J. Hydrol., 200, 24–39, 1997.

Anyah, R. O. and Semazzi, F. H. M.: Variability of East African rainfall based on multiyear RegCM3 simulations, Int. J. Climatol., 27, 357–371, 2007.

Camberlin, P., Janicot, S., and Poccard, I.: Seasonality and atmospheric dynamics of the teleconnection between African rainfall and tropical sea surface temperature: Atlantic vs. ENSO, Int. J. Climatol., 21, 973–1005, 2001.

Chen, T. C. and van Loon, H.: Interannual variation of the tropical easterly jet, Mon. Weather Rev., 115, 1739–1759, 1987.

Cook, K. H.: Generation of the African easterly jet and its role in determining West African precipitation, J. Climate, 12, 1165–1184, 1999.

Coppola, E., Giorgi, F., Mariotti, L., and Bi, X.: RegT-Band: A tropical band version of RegCM4, Clim. Res., 52, 115–133, 2012.

D'Amato, N. and Lebel, T.: On the characteristics of the rainfall events in the Sahel with a view to the analysis of climatic variability, Int. J. Climatol., 18, 955–974, 1998.

Dee, D. P., Uppala, S. M., Simmons, A. J., Berrisford, P., Poli, P., Kobayashi, S., Andrae, U., Balmaseda, M. A., Balsamo, G., Bauer, P., Bechtold, P., Beljaars, A. C. M., van de Berg, L., Bidlot, J., Bormann, N., Delsol, C., Dragani, R., Fuentes, M., Geer, A. J., Haimberger, L., Healy, S. B., Hersbach, H., Hólm, E. V., Isaksen, L., Kållberg, P., Köhler, M., Matricardi, M., McNally, A. P., Monge-Sanz, B. M., Morcrette, J. J., Park, B. K., Peubey, C., de Rosnay, P., Tavolato, C., Thépaut, J. N., and Vitart, F.: The ERA-Interim reanalysis: configuration and performance of the data assimilation system, Q. J. Roy. Meteor. Soc., 137, 553–597, doi:10.1002/qj.828, 2011.

De Putter, T., Loutre, M., and Wansard, G.: Decadal periodicities of Nile River historical discharge (AD 622–1470) and climatic implications, Geophys. Res. Lett., 25, 3193–3196, 1998.

Dickinson, R. E., Henderson-Sellers, A., Kennedy, P. J., and Wilson, M. F.: Biosphere–atmosphere transfer scheme (BATS) version 1e as coupled to the NCAR Community Climate Model, NCAR Tech. Note, NCAR/TN387+ STR., 1993.

HESSD
11, 2233–2262, 2014

Druyan, L. M., Fulakeza, M., and Lonergan, P.: The impact of vertical resolution on regional model simulation of the west African summer monsoon, Int. J. Climatol., 28, 1293–1314, 2008.
Dumont, H. J. (Ed.): The Nile, in: Origin, environments, limnology and human use, Monog. Biol., Vol. 89, Springer Netherlands, 2009.
Elagib, N. A. and Elhag, M. M.: Major climate indicators of ongoing drought in Sudan, J. Hydrol., 409, 612–625, 2011.
Eltahir, E. A. B.: El Niño and the natural variability in the flow of the Nile River, Water Res. Res., 32, 131–137, 1996.
Emanuel, K.: A scheme for representing cumulus convection in large-scale models, J. Atmos. Sci., 48, 2313–2335, 1991.
Flaounas, E., Bastin, S., and Janicot, S.: Regional climate modelling of the 2006 West African monsoon: sensitivity to convection and planetary boundary layer parameterisation using WRF, Clim. Dynam., 36, 1083–1105, 2011.
Fontaine, B. and Janicot, S.: Wind-field coherence and its variations over West Africa, J. Climate, 5, 512–524, 1992.
Gallée, H., Moufouma-Okia, W., Bechtold, P., Brasseur, O., Dupays, I., Marbaix, P., Messager, C., Ramel, R., and Lebel, T.: A high resolution simulation of a West African rainy season using a regional climate model, J. Geophys. Res., 109, D05108, doi:10.1029/2003JD004020, 2004.
Giorgi, F., Coppola, E., Solmon, F., Mariotti, L., Sylla, M. B., Bi, X., Elguindi, N., Diro, G. T., Nair, V., and Giuliani, G.: RegCM4: model description and preliminary tests over multiple CORDEX domains, Clim. Res., 52, 7–29, doi:10.3354/cr01018, 2012.
Gissila, T., Black, E., Grimes, D. I. F., and Slingo, J. M.: Seasonal forecasting of the Ethiopian summer rains, Int. J. Climatol., 24, 1345–1358, 2004.
Grell, G. A.: Prognostic evaluation of assumptions used by cumulus parameterizations, Mon. Weather Rev., 121, 764–787, 1993.
Holtslag, A. A. M., De Bruijn, E. I. F., and Pan, H. L.: A high resolution air mass transformation model for short-range weather forecasting, Mon. Weather Rev., 118, 1561–1575, 1990.
Huffman, G. J., Bolvin, D. T., and Adler, R. F.: GPCP Version 2.2 Combined Precipitation Data set, WDC-A, NCDC, Asheville, NC, available at: http://www.ncdc.noaa.gov/oa/wmo/wdcamet-ncdc.html (last access: October 2011), 2011.

HESSD
11, 2233–2262, 2014

Jenkins, G. S., Gaye, A. T., and Sylla, B.: Late 20th century attribution of drying trends in the Sahel from the Regional Climate Model (RegCM3), Geophys. Res. Lett., 32, L22705, doi:10.1029/2005GL024225, 2005.

Kiehl, J. T., Hack, J. J., Bonan, G. B., Boville, B. A., Briegleb, B. P., Williamson, D. L., and Rasch, P. J.: Description of the NCAR Community Climate Model (CCM3), NCAR Technical Note NCAR/TN-420+STR, doi:10.5065/D6FF3Q99, 1996.

Koteswaram, P.: The Easterly Jet Stream in the tropics, Tellus, 10, 43–57 1958.

Mitchell, T. D., Carter, T. R., Jones, P. D., Hulme, M., and New, M.: A comprehensive set of high-resolution grids of monthly climate for Europe and the globe: the observed record (1901–2000) and 16 scenarios (2001–2100), Tyndall Centre for Climate Change Research Working Paper, 55, 25 pp., 2004.

Müller, W. A. and Roeckner, E.: ENSO teleconnections in projections of future climate in ECHAM5/MPI-OM, Clim. Dynam., 31, 533–549, 2008.

Nikulin, G., Jones, C., Samuelsson, P., Giorgi, F., Sylla, M. B., Asrar, G., Baüchner, M., Christensen, O. B., Déqué, M., and Fernandez, J.: Precipitation climatology in an ensemble of CORDEX-Africa regional climate simulations, J. Climate, 25, 6057–6078, doi:10.1175/JCLI-D-11-00375.1,2012.

Osman, Y. Z. and Shamseldin, A. Y.: Qualitative rainfall prediction models for central and southern Sudan using El Niño–Southern Oscillation and Indian Ocean sea surface temperature indices, Int. J. Climatol., 22, 1861–1878, 2002.

Osman, Y. Z., Shamseldin, A. Y., and Abdo, G. M.: El Niño-Southern Oscillation and rainfall variability in central and southern Sudan, Water Int., 26, 177–184, 2001.

Paeth, H., Born, K., Podzun, R., and Jacob, D.: Regional dynamical downscaling over West Africa: model evaluation and comparison of wet and dry years, Meteorol. Z., 14, 349–368, 2005.

Pal, J. S., Eltahir, E. A. B., and Small, E. E.: Simulation of regional-scale water and energy budgets: Representation of subgrid cloud and precipitation processes within RegCM, J. Geophys. Res., 105, 567–594, 2000.

Pal, J. S., Giorgi, F., Bi, X., Elguindi, N., Solmon, F., Rauscher, S. A., Gao, X., Francisco, R., Zakey, A., and Winter, J.: Regional climate modeling for the developing world: the ICTP RegCM3 and RegCNET, B. Am. Meteorol. Soc., 88, 1395–1409, 2007.

HESSD
11, 2233–2262, 2014

Reynolds, R. W., Smith, T. M., Liu, C., Chelton, D. B., Casey, K. S., and Schlax, M. G.: Daily high-resolution-blended analyses for sea surface temperature, J. Climate, 20, 5473–5496, 2007.
Segele, Z. T. and Lamb, P. J.: Characterization and variability of Kiremt rainy season over Ethiopia, Meteorol. Atmos. Phys., 89, 153–180, 2005.
Seleshi, Y. and Zanke, U.: Recent changes in rainfall and rainy days in Ethiopia, Int. J. Climatol., 24, 973–983, 2004.
Shukla, J., Marx, L., Paolino, D., Straus, D., Anderson, J., Ploshay, J., and Kalnay, E.: Dynamical seasonal prediction, B. Am. Meteorol. Soc., 81, 2593–2606, 2000.
Steiner, A. L., Pal, J. S., Rauscher, S. A., Bell, J. L., Diffenbaugh, N. S., Boone, A., Sloan, L. C., and Giorgi, F.: Land surface coupling in regional climate simulations of the West African monsoon, Clim. Dynam., 33, 869–892, 2009.
Sun, L., Semazzi, F. H. M., Giorgi, F., and Ogallo, L. A.: Application of the NCAR regional climate model to eastern Africa. Part 1: simulation of the short rains of 1988, J. Geophys. Res., 104, 6529–6548, 1999.
Sylla, M. B., Dell'Aquila, A., Ruti, P. M., and Giorgi, F.: Simulation of the intraseasonal and the interannual variability of rainfall over West Africa with RegCM3 during the monsoon period, Int. J. Climatol., 30, 1865–1883, 2010a.
Sylla, M. B., Coppola, E., Mariotti, L., Giorgi, F., Ruti, P. M., Dell'Aquila, A., and Bi, X.: Multiyear simulation of the African climate using a regional climate model (RegCM3) with the high resolution ERA-interim reanalysis, Clim. Dynam., 35, 231–247, 2010b.
Thorncroft, C. D. and Blackburn, M.: Maintenance of the African easterly jet, Q. J. Roy. Meteor. Soc., 125, 763–786, 1999.
Vizy, E. K. and Cook, K. H.: Development and application of a mesoscale climate model for the tropics: Influence of sea surface temperature anomalies on the West African monsoon, J. Geophys. Res., 107, ACL 2-1–ACL 2-22, doi:10.1029/2001JD000686, 2002.
Wang, G. and Eltahir, E. A. B.: Use of ENSO information in medium-and long-range forecasting of the Nile floods, J. Climate, 12, 1726–1737, 1999.
Wu, M. L. C., Reale, O., Schubert, S. D., Suarez, M. J., Koster, R. D., and Pegion, P. J.: African Easterly Jet: Structure and Maintenance, J. Climate, 22, 4459–4480, 2009.
Zaroug, M. A. H., Eltahir, E. A. B., and Giorgi, F.: Droughts and floods over the upper catchment of the Blue Nile and their connections to the timing of El Niño and La Niña Events, Hydrol. Earth Syst. Sci. Discuss., 10, 10971–10995, doi:10.5194/hessd-10-10971-2013, 2013.

HESSD
11, 2233–2262, 2014

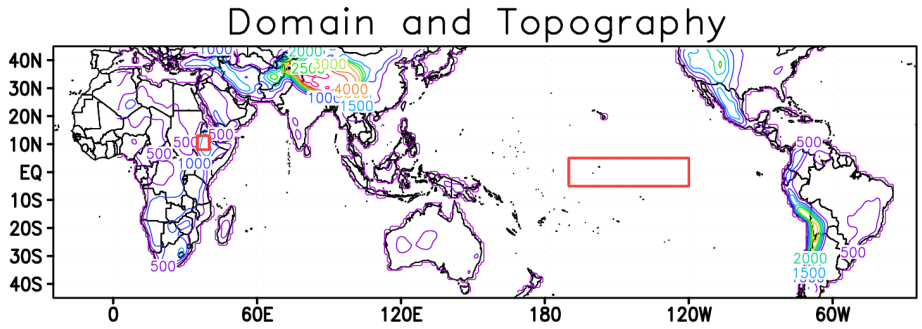

Fig. 1. The domain and the topography of the model. The red box in the Pacific Ocean illustrated Nino 3.4 region, and the red box in Ethiopian Highland illustrated the upper catchment of the Blue Nile.

HESSD
11, 2233–2262, 2014

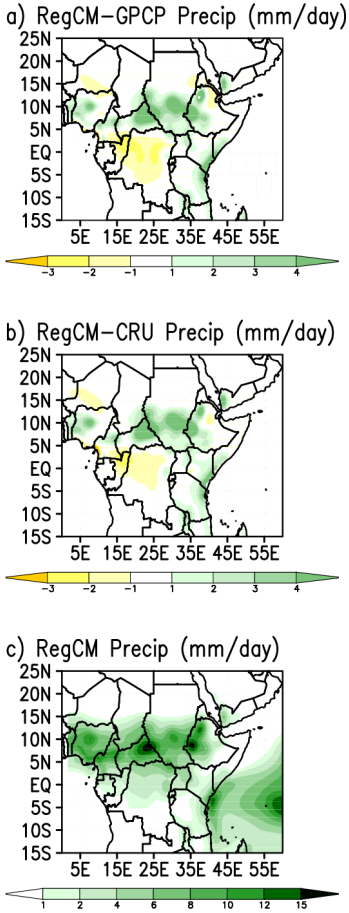

Fig. 2. Averaged precipitation (in mm day^{-1}) for JJAS 1982–2009: **(a)** RegCM minus CRU, **(b)** RegCM minus GPCP, and **(c)** RegCM.

HESSD
11, 2233–2262, 2014

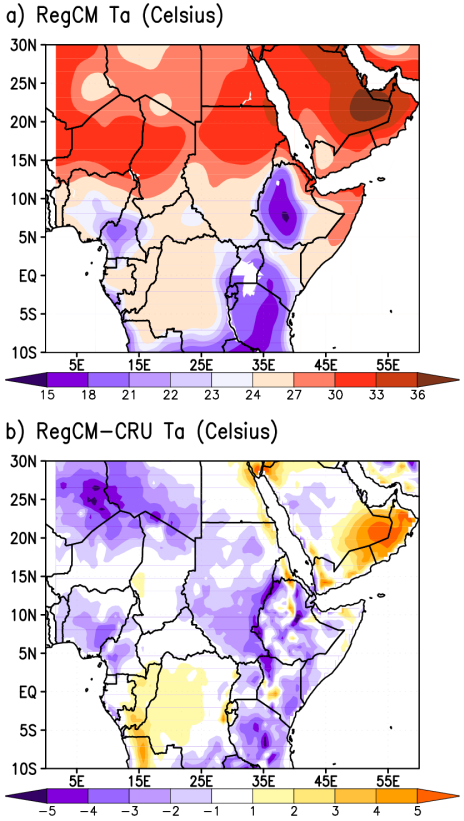

Fig. 3. Averaged 2 m air temperature (in C) for JJAS 1982–2009: **(a)** RegCM, **(b)** RegCM minus CRU.

HESSD
11, 2233–2262, 2014

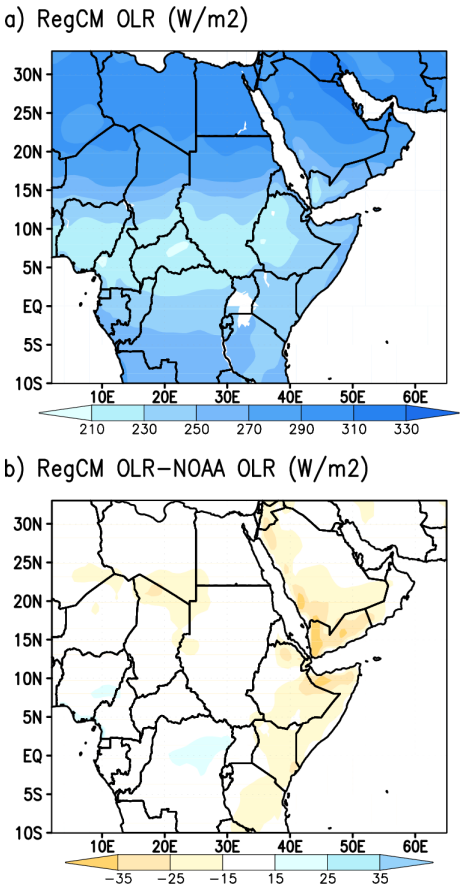

Fig. 4. Averaged outgoing longwave radiation (in $W m^{-2}$) for JJAS 1982–2009: **(a)** RegCM OLR, **(b)** RegCM OLR minus NOAA OLR.

HESSD
11, 2233–2262, 2014

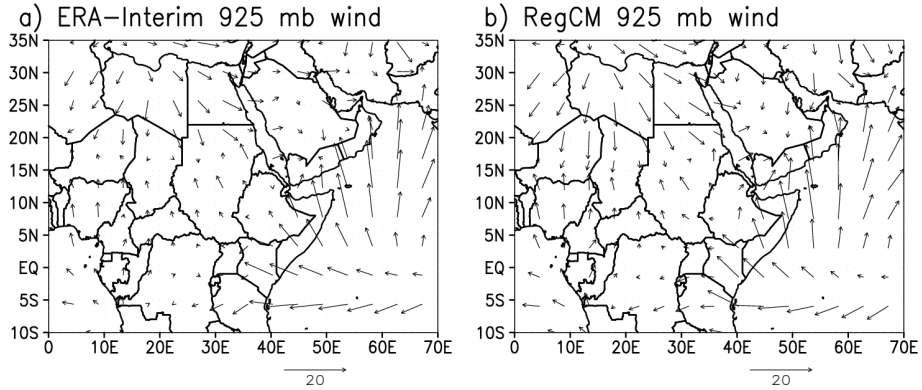

Fig. 5. The black arrows show the averaged 925 mb wind vector for JJA 1982–2009: **(a)** ERA-Interim, **(b)** RegCM.

HESSD
11, 2233–2262, 2014

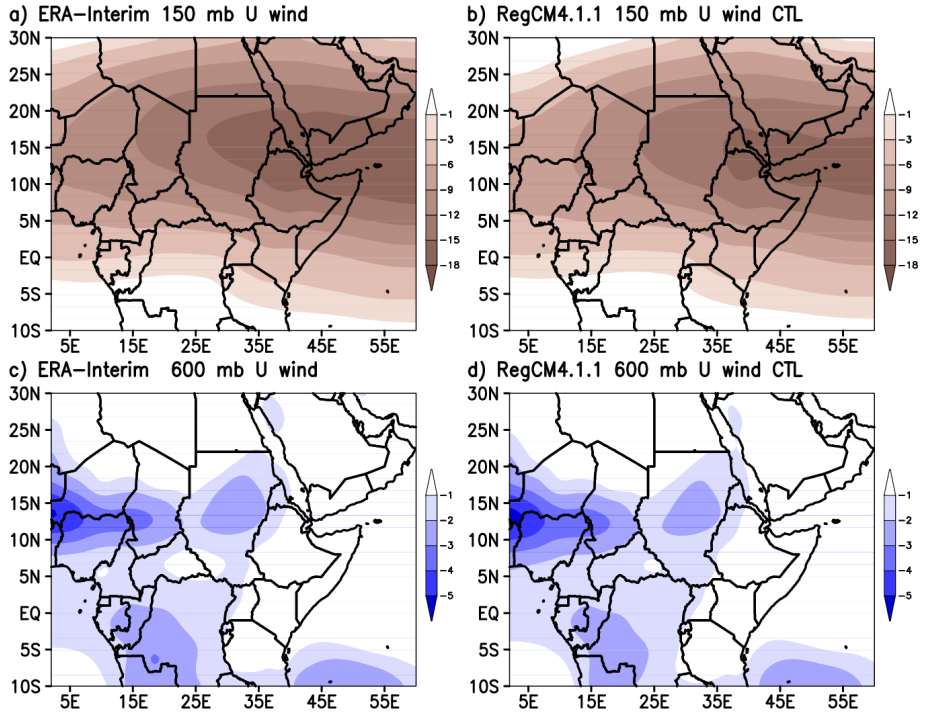

Fig. 6. Averaged zonal wind (in $m s^{-1}$) for JJAS 1982–2009: **(a)** ERA Interim at 150 mb, **(b)** RegCM at 150 mb, **(c)** ERA Interim at 600 mb, and **(d)** RegCM at 600 mb.

HESSD
11, 2233–2262, 2014

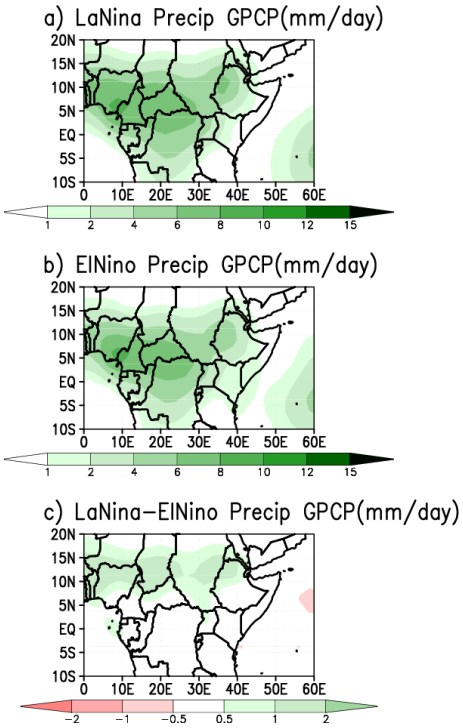

Fig. 7. The rainfall in North Africa from GPCP during JJAS for **(a)** 5 La Niña years (88,98, 99, 07, and 08), **(b)** 5 El Niño years (82, 83, 87, 92, and 02), and **(c)** the difference between La Niña years and El Niño years.

HESSD
11, 2233–2262, 2014

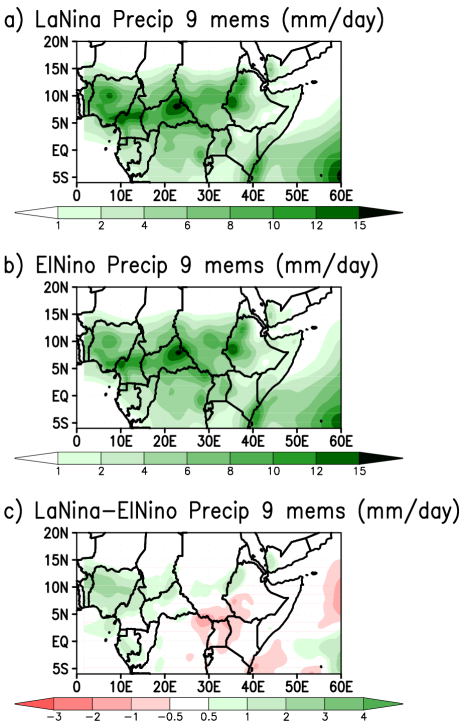

Fig. 8. The rainfall in North Africa from 9 average members during JJAS for **(a)** 5 La Niña years (88, 98, 99, 07, and 08), **(b)** 5 El Niño years (82, 83, 87, 92 and 02), and **(c)** the difference between La Niña years and El Niño years.

HESSD
11, 2233–2262, 2014

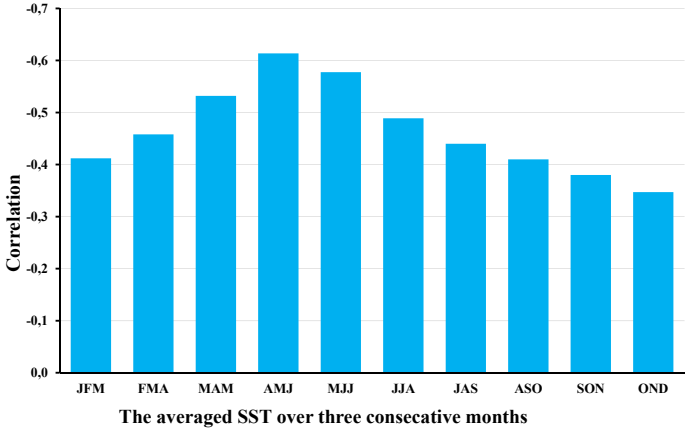

Fig. 9. The correlation between rainfall anomalies over Ethiopian Highlands for 9 averaged members and SST anomalies over the Pacific Ocean in Nino 3.4 region.

HESSD
11, 2233–2262, 2014

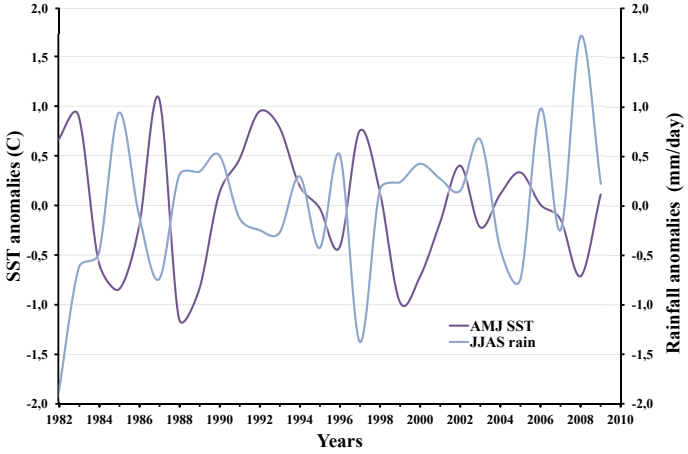

Fig. 10. The SST anomalies during AMJ in Nino 3.4 region and the rainfall anomalies in the upper catchment of the Blue Nile for 9 averaged members.

HESSD
11, 2233–2262, 2014

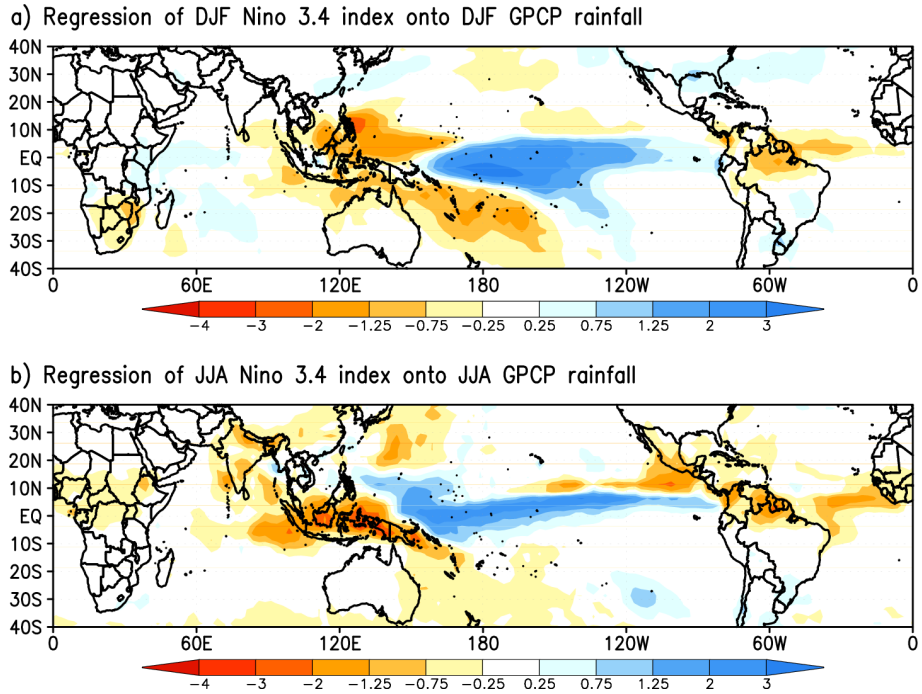

Fig. 11. Regression of DJF and JJA of Nino 3.4 index onto DJF and JJA for GPCP rainfall for 1982–2009.

HESSD
11, 2233–2262, 2014

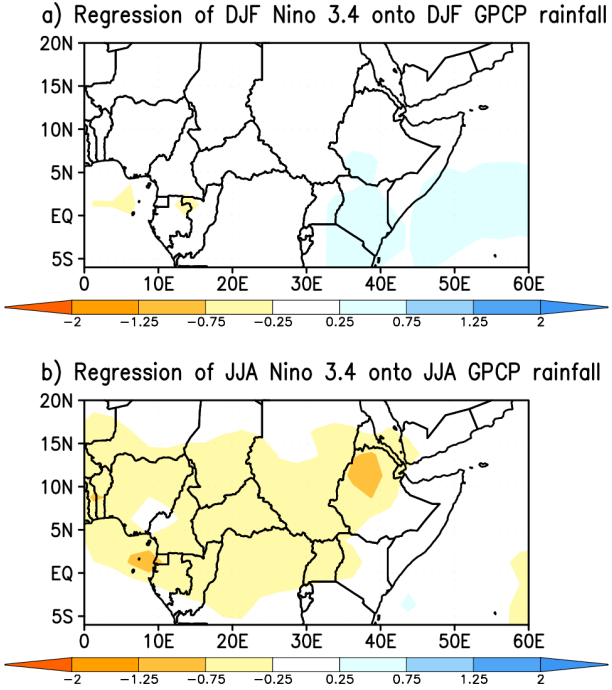

Fig. 12. Regression of DJF and JJA of Nino 3.4 index onto DJF and JJA for GPCP rainfall for (1982–2009) in North Africa.

HESSD
11, 2233–2262, 2014

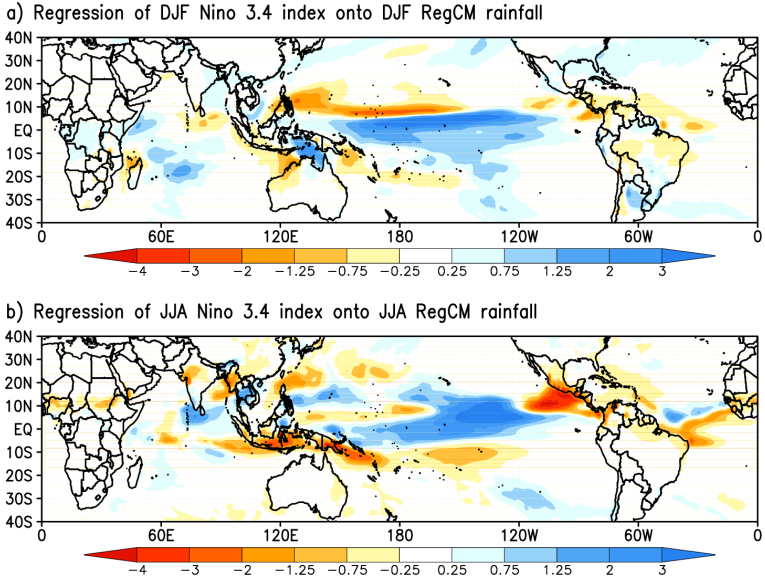

Fig. 13. Regression of DJF and JJA of Nino 3.4 index onto DJF and JJA rainfall for 9 averaged members for (1982–2009).

HESSD
11, 2233–2262, 2014

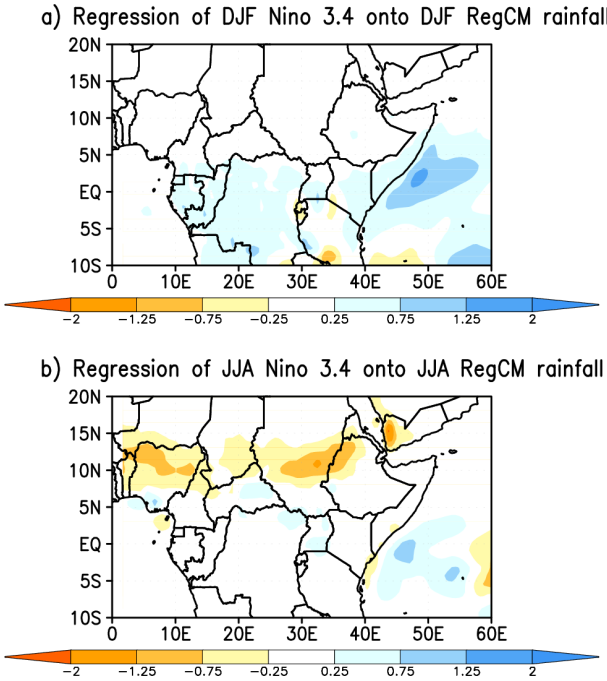

Fig. 14. Regression of DJF and JJA of Nino 3.4 index onto DJF and JJA rainfall for 9 averaged members for (1982–2009) in North Africa.

HESSD
11, 2233–2262, 2014